Physical modeling on large diameter piles subjected to one-way cyclic loading in dense sand focusing on generalized scaling law

Y. Lao
Doctoral Student, Civil and Environmental Engineering, Tokyo Institute of Technology, Tokyo, Japan
J. Takemura
Associate Professor, Civil and Environmental Engineering, Tokyo Institute of Technology, Tokyo, Japan
K. Takeuchi
Engineer, Civil Engineering Design Department, Taisei Corporation, Tokyo, Japan

ABSTRACT

To meet the growing demand for offshore wind turbine (OWT) dimensions and to study the applicability of the Generalized Scaling Law (GSL) on the soil-structural interaction (SSI) of laterally loaded single piles, up to 4m in diameter, targeting the offshore environment, this study presents a series of physical experiments in centrifuge modeling. The nine model piles have an identical diameter and embedded depth but varying wall thicknesses and centrifuge accelerations tailored to create three pile-soil relative stiffness (E_e/G^*) values in the centrifuge environment. The mechanical behaviors, such as the horizontal load-displacement relationship and bending moment profile, are examined on both centrifuge scaling law and GSL, considering the influence of pile-soil relative stiffnesses (E_e/G^*) and structural failure. The results show that the applicability of GSL depends on the level of soil strain along the pile as well as structural yielding. At a small pile top displacement, such as 1% of the pile diameter, GSL shows acceptable accuracy. However, as μ (1G scaling factor) increases, the lateral resistance of the single pile tends to be underestimated before structural failures, indicating the limitation of GSL's core assumption on the scaling factor of strain ($\lambda_\varepsilon=\mu^{0.5}$). This limitation is especially prominent for relatively rigid piles.

Key words: *Centrifuge modelling, Offshore wind turbine, Single pile, Generalized scaling law, Sandy soil.*

1. Introduction

To support the increasing capacity of OWTs, monopile foundations and jacket piles have been adopting larger diameters recently. The monopile foundations, for example, are pushing more than 8m in diameter (Aranya et al., 2017). Physical modeling, especially centrifuge models in many studies (e.g., Klinkvort et al., 2013 & 2018), have extensively researched these foundations. The challenge is that modeling the significant loading eccentricity in OWT designs requires larger diameters for model piles, potentially surpassing the rotating platform's arm length. Therefore, it is relevant to examine the reliability and applicability of various existing scaling laws on offshore pile foundations.

Iai (2005) and Tobita (2011 & 2016) proposed a generalized scaling law (GSL) that allows the modeling of large-scale prototypes in a small-scale centrifuge through the combination (λ) of centrifuge (η, unit: g) and 1G scaling laws (μ). However, due to the complexity of SSI under horizontal loading, the core assumptions made by Iai regarding the stress-dependent soil stiffness and strain ($\lambda_\varepsilon=\mu^{0.5}$) in 1G scaling laws induce uncertainties about the applicability of GSL. Furthermore, the complexity is exacerbated the variation of nonlinearity with depth, which are mainly determined by 1) relative stiffness of pile and soil; 2) pile embedment to diameter ratio (d_e/Φ).

To provide reliable experimental evidence and analysis to support more efficient designs for OWTs, this study aims to discuss the applicability of GSL on single piles by analyzing nine centrifuge tests with different t/D ratios, categorized by three different E_e/G^* values.

2. Centrifuge model tests

This study is centered around centrifuge modeling of steel tubular pile foundation in sand, as depicted in **Figure 1**. The experimental setup is shown in **Figure 2**. The structural and geotechnical factors, namely stiffnesses and strengths of pile and soil, should be individually controlled. In this study, the variation of pile stiffness was achieved by three model piles with the same Φ but different t (**Figure 3**). With proper combination of η and virtual 1G scaling factor (μ), the test results will be discussed by the centrifugal scaling law and GSL. Three model grounds with three piles each were created, totaling nine pile loading sessions conducted under different η values. These values were set to ensure an identical pile diameter in each model on GSL scale: 1m, 2m, and 4m. Test conditions are summarized in **Table 1**.

A gradually-increased-one-way cyclic loading session was applied to each pile 50mm above ground. The model piles were laterally loaded from small (allowable limit) to large displacements (ultimate limit). Across the cases, the tests kept the same sand type, relative density, pile type, length, diameter, embedment ratio, and loading height.

2.1. Model ground and piles

The model was dry Toyoura sand (**Table 2**) and had a relative density (Dr.) of 80%. Sand was filled up to 145mm from the bottom and leveled. Then, the pile was fixed with only 15mm of length buried in sand. After that, more sand was added to have pile embedment depth, d_e=260mm (d_e/Φ=6.5) and leveled again.

2.2. Applied loads and measurements

This study uses displacement-controlled one-way cyclic loadings (example: **Figure 4**). The following were measured during the loading: the horizontal movement of the pile at the load point (δ_t), the horizontal movement of the pile 30mm above the load point, the applied lateral load (P_L), the jack stroke, and the bending moment calculated from the strain gauge, as shown in **Figure 2**.

After unloading from δ_t=6mm (15% of Φ), the pile was loaded extensively until the peak load was observed.

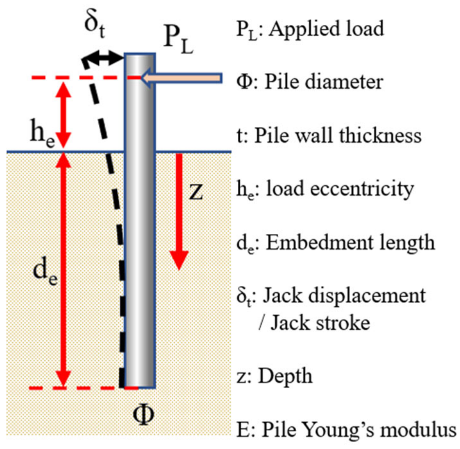

Figure 1: Parameters of single pile

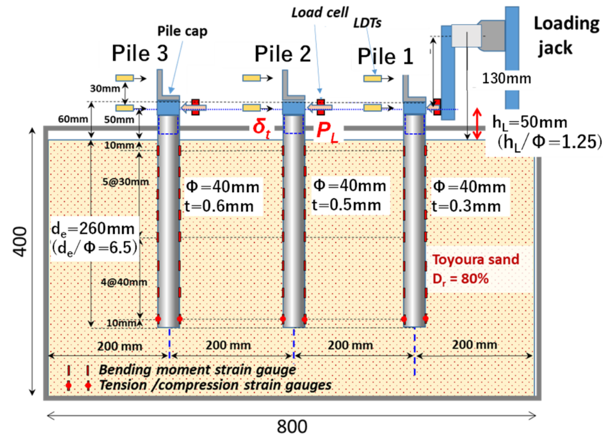

Figure 2: Schematic diagram of experimental setup

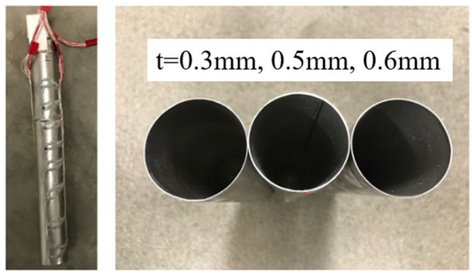

Figure 3: Model piles used

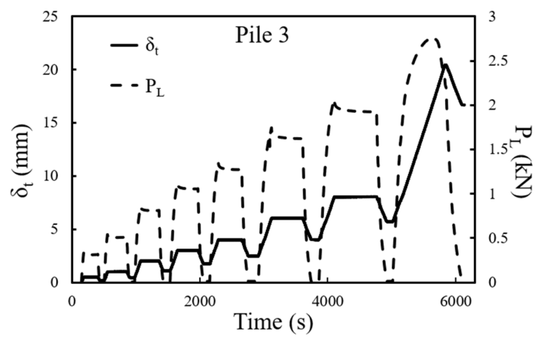

Figure 4: Time series of applied force and displacement of Pile 3

Table 1: Test cases and conditions

Model 1	Pile 1	Pile 2	Pile 3
Thickness t (mm)	0.3	0.5	0.6
Diameter Φ (mm)	40		
t/ Φ	0.0075	0.0125	0.015
Centrifuge η (g)	6.55	17.6	25
Diameter Φ [m]	[0.26]	[0.7]	[1]
μ	3.8	1.4	1
Diameter Φ {m}	{1}		
EI ($kN.m^2$) {GN. m^2}	1.45{1.11}	2.38 {1.11}	2.84{1.11}
M_y (N.m) {MN.m}	94 {5.6}	154 {3.4}	184 {2.9}
Model 2	Pile 4	Pile 5	Pile 6
Thickness (mm)	0.3	0.5	0.6
Diameter Φ (mm)	40		
t/ Φ	0.0075	0.0125	0.015
Centrifuge η (g)	13.1	35.3	50
Diameter Φ [m]	[0.5]	[1.4]	[2]
μ	3.8	1.4	1
Diameter Φ {m}	{2}		
EI ($kN.m^2$) {GN. m^2}	1.45{17.4}	2.38{17.4}	2.84{17.4}
M_y (N.m) {MN.m}	94 {44.8}	154 {27.3}	184 {23}
Model 3	Pile 7	Pile 8	Pile 9
Thickness (mm)	0.3	0.5	0.6
Diameter Φ (mm)	40		
t/ Φ	0.0075	0.0125	0.015
Centrifuge η (g)	26.2	70.6	100
Diameter Φ [m]	[1]	[2.8]	[4]
μ	3.8	1.4	1
Diameter Φ {m}	{4}		
EI ($kN.m^2$) {GN. m^2}	1.45{278}	2.38{278}	2.84{278}
M_y (N.m) {MN.m}	94 {359}	154 {219}	184 {184}
d_e/Φ for all piles	6.5		

Note. Numbers in "[]" are on centrifuge scale. Numbers in "{}" are on GSL scale.

2.3. Pile-soil relative stiffnesses (E_e/G^*)

To evaluate the effects of pile, Randolph (1981) used a relative moduli parameter, E_e/G^*, which is a stiffness parameter that combines the pile stiffness coefficient and the ground stiffness coefficient (Randolph, M. F., 1978). E_e is the effective stiffness coefficient of the pile and can be expressed as **Equation (1)** using the bending stiffness (EI) of the pile and Φ.

On the same model sand condition, E_e/G^* of each pile can be different depending on the pile wall thickness, η, and the stress dependency of soil stiffness. G* is a parameter representing the rigidity of the ground, which depends on the ground shear stiffness G and Poisson's ratio ν. The void ratio e is 0.6794. The calculation of ground shear stiffness G is estimated by Iwasaki et al. (1978).

$$E_e = \frac{64EI}{\pi\Phi^4} \tag{1}$$

$$G^* = G(1 + 3\nu/4) \tag{2}$$

$$\{G\}_{\gamma,p} = K(\gamma)\frac{(2.17-e)^2}{1+e}p^{m(\gamma)} \tag{3}$$

where p is the mean effective stress, and K(γ) and m(γ) are functions of the shear strain γ. **Figure 5** gives the relationship between G and void ratio e with p fixed at 1.0. Subsequently, for the given e and the assumed γ, K(γ) was obtained.

The value m(γ) represents the effect of γ on the stress dependency of stiffness, as shown in **Figure 6**. it should be noted that variation of m(γ) is rather small (0.4~0.5) for γ less than 10^{-4}. The mean effective stress p, expressed with the vertical stress σ_a and the horizontal stress σ_r, can be determined by the following equations:

$$p = \frac{\sigma_a' + 2\sigma_r'}{3} \tag{4}$$

$$\sigma_a' = \gamma_d z \tag{5}$$

$$\sigma_r' = K_0\gamma_d z \tag{6}$$

where K_0 is the at-rest earth pressure coefficient = 0.34, γ_d the dry unit weight of the soil = 15.5kN/m^3.

This definition of G means that its values vary with the ground depth and the assumed γ, as shown in **Figure 7**. However, regarding G and γ, it is worth noting that no universally recognized recommendations yet exist. In this study, as a reference for relatively small strain level, G is determined assuming the p at z/Φ=2, γ=10^{-4} i.e., m(γ)=0.5. The value G* representing the stiffness of the soil can therefore be obtained by **Equations (2)** and **(3)**.

Noted that in the recommended p-y lateral loading capacity calculation by API (2014), the depth factor "A" decreases until z/Φ=2.5, marking the critical depth. The API model was built on laterally loaded flexible piles of which the shallow depth is governed by wedge failure that, at the critical depth z/Φ=2.5, transitions to circumferential failure in the horizontal plane. Conversely, monopiles of all diameters exhibit a deep wedge failure mode in the upper section of the pile with rotational soil flow in the vertical plane below this section (Wang et al., 2023).

To ensure that E_e/G^* values are relevant for monopile foundations, G should be determined at depths shallower than the critical depth. In addition, the reliability of the API-suggested z/Φ=2.5 for all scenarios is unknown. Based on the above information, this study uses a slightly shallower z/Φ=2 to determine shear modulus G for calculating E_e/G^*.

At z=2×Φ in the model, p is proportional to η, thus the combination of model pile EI and η determines the E_e/G^* values. **Figure 8** plots the E_e/G^* values of nine piles against relative pile embedment ratio for $\gamma=10^{-4}$ and 3×10^{-3}. As the η values of piles in each model ground were determined to have the same prototype pile diameter on GSL scale, which assumes the stiffness is proportional to the square root of p, the E_e/G^* for $\gamma=10^{-4}$ ($m(\gamma)=0.5$) are equal in each model. But for $\gamma=3\times10^{-3}$, different E_e/G^* values are obtained.

2.4. Generalized scaling factors

One of the core assumptions in GSL is that the model soil stiffness should be multiplied by $\mu^{0.5}$ to get the prototype one (Iai et al., 2005), and therefore the scaling GSL factor of EI is $\mu^{4.5}\eta^4$, as shown in **Table 3**. In **Table 1**, when μ=1, centrifuge scaling is applied to the corresponding case, not GSL. It is important to note that, according to GSL, the prototype pile yielding bending moment (M_y) is scaled to be greater for the model pile with the larger μ value.

3. Test results and discussion

3.1. Centrifuge scaling

The lateral load-displacement (P_L-δ_t) relations obtained from the nine centrifuge model tests are shown in **Figure 9**. The P_L-δ_t curves of pile 3 to 9 in model scale show signs of buckling towards the end. However, it can be observed that Piles 1 and 2 did not reach structural failure during the experiment. The results are also plotted in centrifuge prototype scale in **Figure 10**.

Table 2: Model materials specifications

Dry density (γ_d)	15.5 kN/m^2
Friction angle (φ’)	41 degrees
Cohesion (c)	0 kN/m^2
Poisson’s ratio (ν)	0.3
Soil particle density (ρ_s)	2.64g/cm^3
Minimum void ratio (e_{min})	0.609
Max void ratio (e_{max})	0.973

Table 3: Generalized scaling factors

	Centrifugal	1G	Generalized
Length: L	η	μ	$\eta\mu$
Area: A	η^2	μ^2	$\eta^2\mu^2$
Volume: V	η^3	μ^3	$\eta^3\mu^3$
Unit weight: γ	$1/\eta$	1	$1/\eta$
Stress: σ	1	μ	μ
Strain: ε	1	$\mu^{0.5}$	$\mu^{0.5}$
Force: F	η^2	μ^3	$\eta^2\mu^3$
Young’ modulus: E	1	$\mu^{0.5}$	$\mu^{0.5}$
Flexural rigidity: EI	η^4	$\mu^{4.5}$	$\eta^4\mu^{4.5}$
Bending Moment: M	η^3	μ^4	$\eta^3\mu^4$

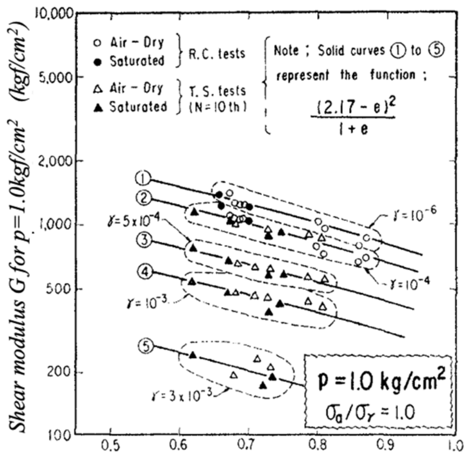

Figure 5: G versus e relationship of Toyoura sand (Iwasaki et al. 1978)

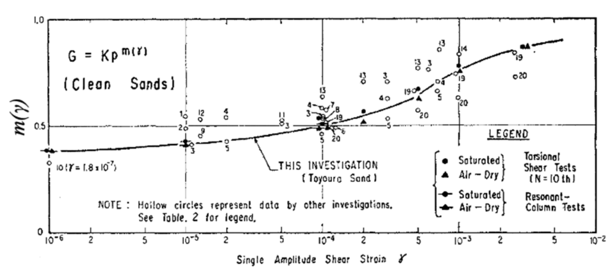

Figure 6: m(γ) versus γ relationship of clean sand (Iwasaki et al. 1978)

Figure 11 depicts P-Φ curves for δ_t/Φ values of 1%, 5%, and 10%. It confirms a direct relationship between pile diameter and load at the same normalized displacements. This relationship approximates a power function described by two parameters, A and α.

$$P = A\phi^{\alpha} \tag{7}$$

where α signifies the load changes with the pile diameter, with higher α values indicating a greater impact of the pile diameter under loading. In **Figure 12**, the P-Φ relationship maps P values at δ_t/Φ= 1%, 5%, and 20%. With both axes in logarithmic scale, the presented data points show linear relations that can be distinguished by the level of δ_t/Φ. Specifically, Difference δ_t/Φ values only seem to alter the Y axis intercept without changing the slope.

According to **Equation (7)**, when Φ= 1m, P_L=A. Because each E_e/G^* level, visually distinguished by colors, shows a near straight-line correlation in logarithmic scale, the resulting A values are considered representative to their corresponding E_e/G^* group. Then, with P, A, and Φ values confirmed, α can also be derived. **Figure 13** plots the change of A and α with E_e/G^*.

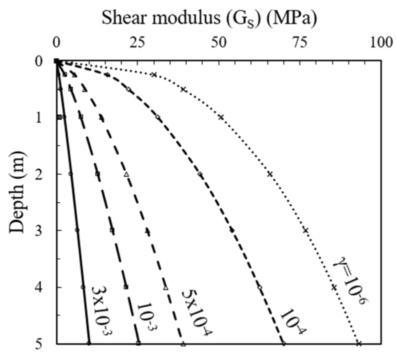

Figure 7: Depth variation of shear moduli for different strain level estimated based on Equation (3)

Table 4: E_e/G^* values in centrifuge

Strain level	Pile 1	Pile 2	Pile 3
0.01%		417	
0.3%	6460	4490	3940
Strain level	Pile 4	Pile 5	Pile 6
0.01%		294	
0.3%	3540	2450	2160
Strain level	Pile 7	Pile 8	Pile 9
0.01%		208	
0.3%	1940	1340	1180

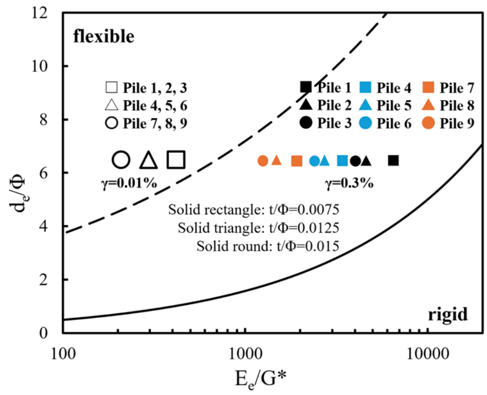

Figure 8: Pile-soil relative stiffnesses (centrifuge scale)

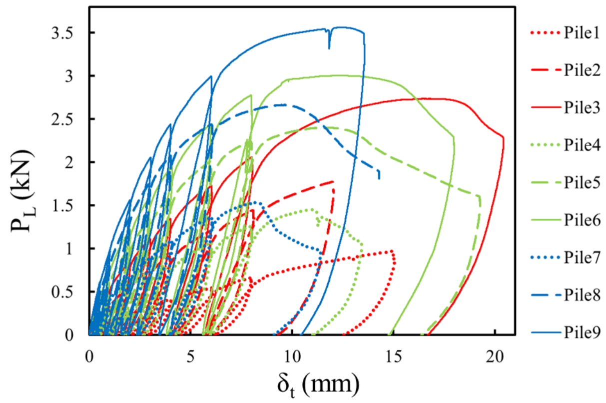

Figure 9: P_L- δ_t For Pile 1 to 9 (Model Scale)

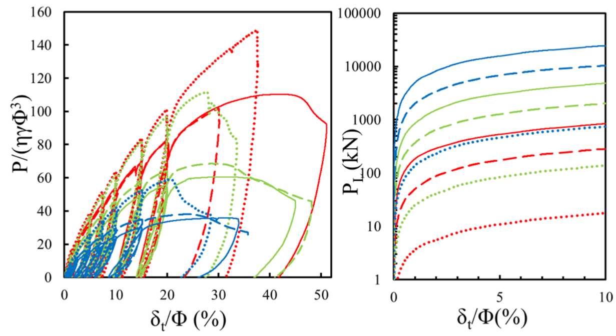

Figure 10: Normalized P_L- δt (Left) (centrifuge Scale) and backbone curves of P_L- δ_t for Pile 1 to 9 (right)

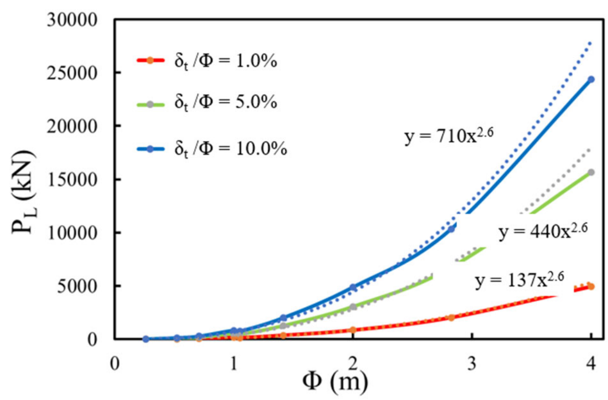

Figure 11: P_L- Φ relations (centrifuge scale)

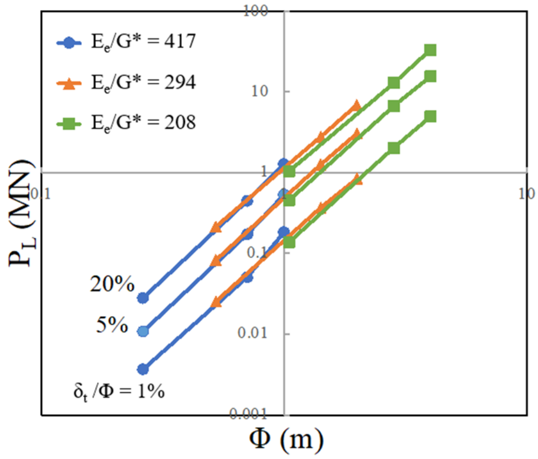

Figure 12: P_L- Φ relations (centrifuge scale)

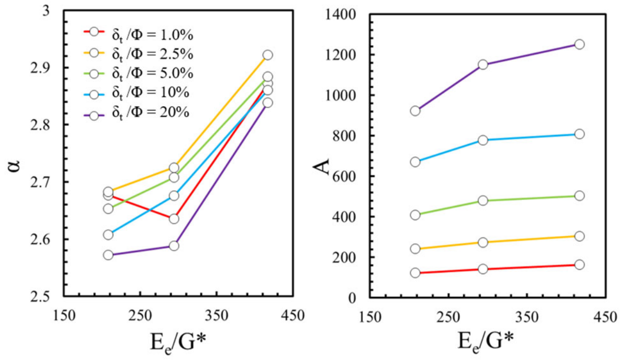

Figure 13: Change of A and α with E_e/G^*

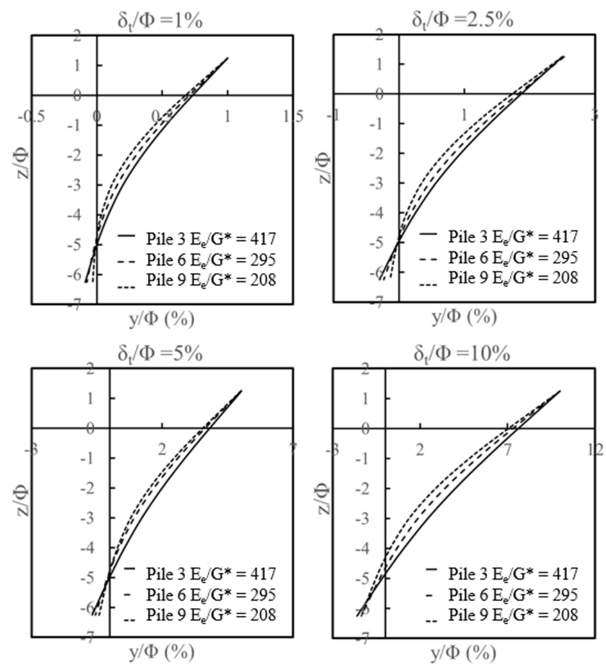

Figure 14: Pile deflection comparisons (GSL applied)

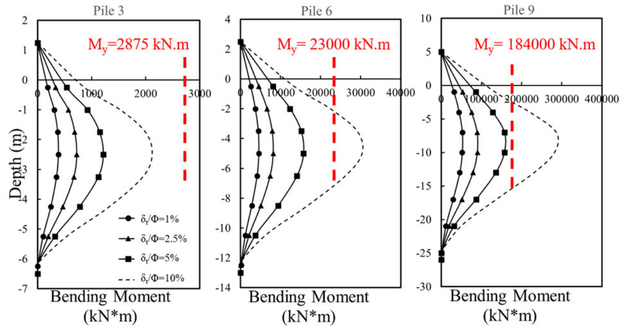

Figure 15: Pile bending moment along the depth

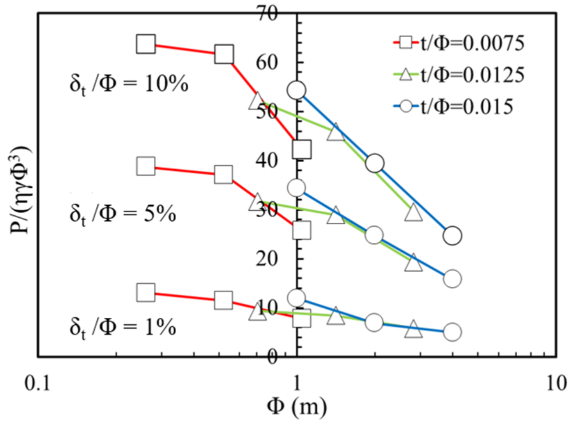

Figure 16: P_L/ ($\eta\gamma\Phi^3$) - Φ relations

Figure 13 shows the α-E_e/G^* and A-E_e/G^* relationships, plotting coefficients A and α at δ_t/Φ=1.0, 2.5, 5, 10, 20% against E_e/G^*. The figure reveals a consistent trend. In the α- E_e/G^* plot, α ranges within about 2.6 to 2.9 and increases with E_e/G^*. A possible explanation can be found in **Figure 14** where the pile deflection comparisons for different E_e/G^* levels are plotted. As expected, for larger pole-soil relative stiffnesses, piles behave more rigid and thus exhibiting straighter deflection profiles in comparison to those of lower E_e/G^* values. This discrepancies in deflection levels influence the shear strain of soil and contributes to the observed trend of α with E_e/G^*.

In the A-E_e/G^* relationship graph, it is evident that A increases with E_e/G^*, particularly for large pile displacements. **Figure 15** depicts bending moment and pile deflection profiles for Piles 3, 6, and 9 at various δt/Φ values across three E_e/G^* levels. Pile 3 exhibits signs of structural failure at δ_t/Φ=2.5%, notably earlier than Piles 6 and 9. This suggests that smaller E_e/G^* leads to yielding with a smaller displacement.

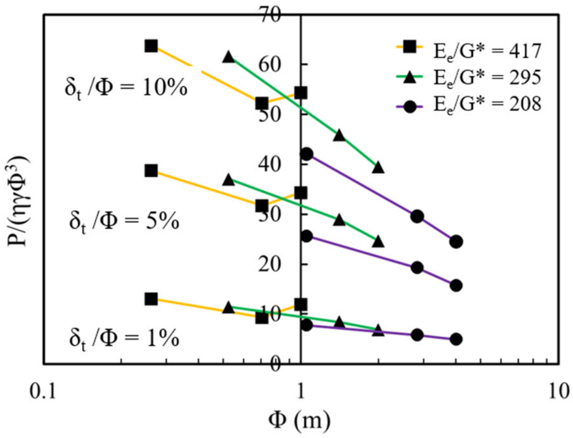

Figure 17: $P_L/(\eta\gamma\Phi^3)$ - Φ relations

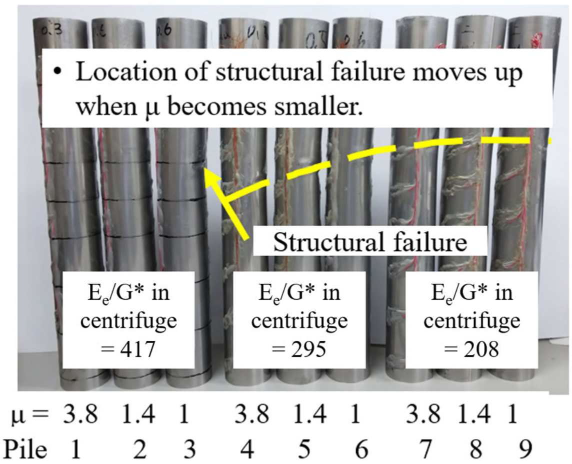

Figure 18: Photo taken after experiment

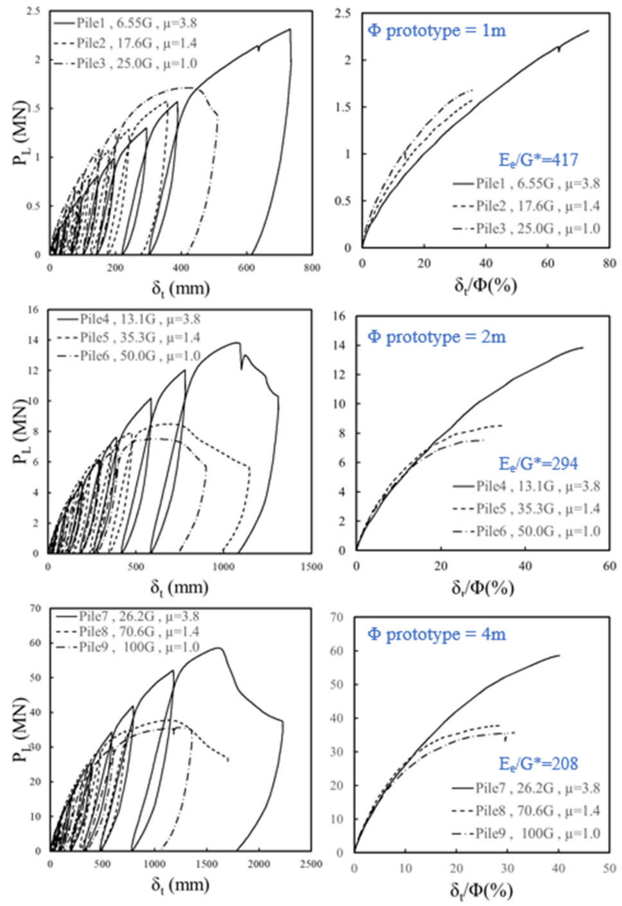

Figure 19: P_L-δ_t/Φ (GSL applied) (left) and the backbone curves of P_L-δ_t/Φ (GSL applied) (right)

To further examine the effect of diameter, **Figure 16** and **17** show the $P_L/(\eta\gamma^3) - \Phi$ relations, categorized by the wall thickness to diameter (t/Φ) ratio and E_e/G^*, with lateral resistance P_L normalized as the Y axis. The decreasing trends can clearly be distinguished by different δt/Φ levels in both figures: 1) For the same δ_t/Φ, the normalized P_L becomes smaller as Φ increases; 2) The larger the δ_t/Φ, the faster the P_L drops.

In **Figure 18**, piles categorized by E_e/G^* show that larger prototype diameter piles within the same E_e/G^* category fail closer to the ground surface. Conversely, piles with smaller E_e/G^* values also exhibit failure nearer to the ground surface.

Higher E_e/G^* values result in piles behaving more like rigid piles, displaying rotational tendencies. In contrast, smaller E_e/G^* values lead to behavior resembling that of a flexible pile. Due to the large stiffness of the ground with respect to piles, failure occurs closer to the ground surface.

3.2. Generalized scaling

In **Table 2**, it can be concluded that, in centrifuge scaling, strain plays no part in the scaling of stiffness.

For soil: $\sigma_{Prototype} = \sigma_{model}$ (8)

For pile: $\lambda_{EI\,prototype} = \lambda_{EI\,model} \times \eta^4$ (9)

But in GSL, strain affects the scaling of displacement and stiffness. When it comes to the GSL scaling factor of strain itself, it is set by Iai et al. (2005) to be $\lambda_\varepsilon=\mu^{0.5}$ based on the small strain behavior of sand.

For soil: $\sigma_{Prototype} = \sigma_{model} \times \mu$ (10)

For pile: $\lambda_{EI\,prototype} = \lambda_{EI\,model} \times \mu^{4.5}\eta^4$ (11)

It means that, per GSL, the soil stress and the flexural rigidity of pile could be overestimated by the 1G scaling factor μ shown in **Equations (10)** and **(11)**. It should be emphasized that that the results of Piles 3, 6, and 9 are presented in centrifuge scale, not GSL, as they serve as reference benchmarks within their respective E_e/G^*. In centrifuge scale, the prototype diameters are 1m, 2m, and 4m for Piles 3, 6, and 9, respectively. Piles 1 and 2 will be scaled to 1m diameter in GSL, Piles 4 and 5 to 2m, and Piles 7 and 8 to 4m.

The primary cause of the foundation's ultimate failure, as observed in **Figures 9** and **10** at the end of the load-displacement curves, was the structural failure of pile. Therefore, higher M_y values are expected to result in greater ultimate resistance for a single pile. This is evident in **Table 1**, where GSL estimates larger M_y values for piles with higher μ, contributing to the higher ultimate resistance exhibited by Piles 1, 4, and 7, which have the largest μ values among all cases. Also, in **Figure 18**, no buckling is observed in Pile 1 (μ=3.4) and 2 (μ=1.8), which is not the case for Pile 3 (μ=1).

Moreover, the overestimation of pile stiffness in larger μ not only affects M_y but also influences structural failure. This is also visible in **Figure 18**, where larger μ models show deeper depths of structural failure due to the relatively smaller soil confinement compared to GSL estimation.

Figure 19 depicts GSL-scaled P_L-δ_t/Φ curves. Despite displacement-controlled loads, piles with μ=3.8 significantly overestimate δt in comparison to **Figure 9**. In GSL, the length scaling factor ημ suggests that the effect of μ is expected to be as prominent as centrifuge acceleration η. This overestimation raises concerns about the reliability of δt in GSL. Consequently, it is advisable to focus on comparing backbone curves rather than the entire "loading" and "unloading" process in the P_L-δ_t/Φ curve. **Figures 19** also plots the backbone curves of the P_L-δ_t/Φ relations, exhibiting alignment to a certain extent when grouped by their respective E_e/G^*.

Figure 20 is the zoomed-in (up to δ_t/Φ=15%) backbone curves shown in **Figure 19**. It helps identifying the range of applicability of GSL. At E_e/G^*=417, the μ=3.8 case (Pile 1) shows almost no agreement with the μ=1.0 case (Pile 3). Conversely, good agreement (up to δ_t/Φ=2%) is observed between the μ=1.4 (Pile 2) and μ=1.0 cases (Pile 3). As E_e/G^* decreases to 294, both μ=3.8 (Pile 4) and μ=1.4 (Pile 5) align well with μ=1.0 (Pile 6) up to δ_t/Φ=2%. The applicability range expands further as E_e/G^* decreases to 208.

Figure 21 shows the bending moment profiles for nine piles with GSL, comparing three piles sharing the same GSL prototype Φ in each subplot. The comparisons are further distinguished by δ_t/Φ values of 1%, 5%, and 10%. The bending moments at yielding (M_y) are marked in the figure. The bending moment profile aids in identifying the onset of yielding or structural failures.

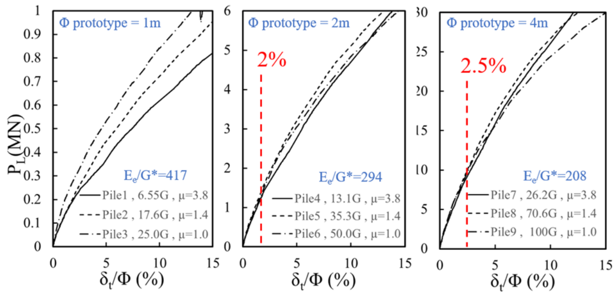

Figure 20: Backbone curves of P_L-δ_t/Φ zoomed in up to δ_t/Φ=15% (GSL applied)

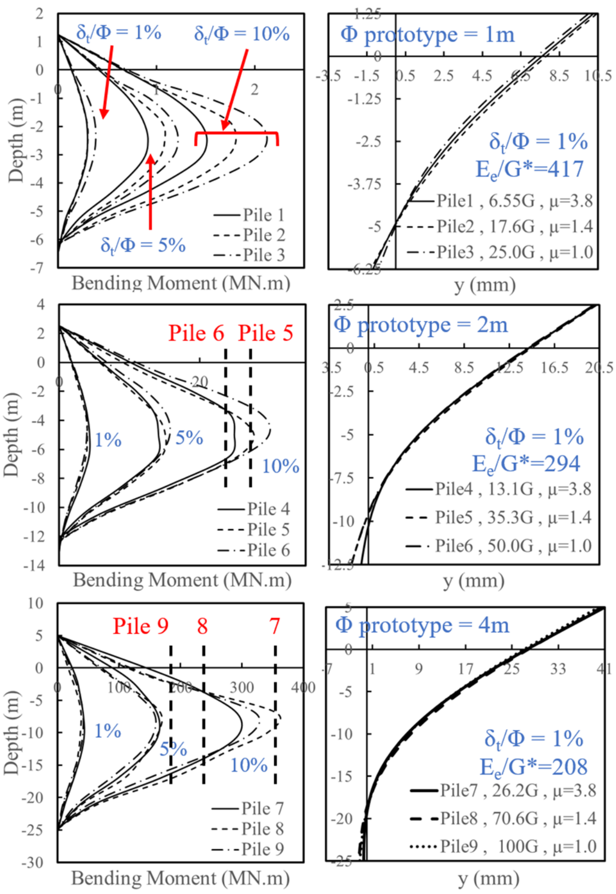

Figure 21: Pile bending moment (left) and deflection at δ_t/Φ=1% (right) profiles along the depth (GSL applied)

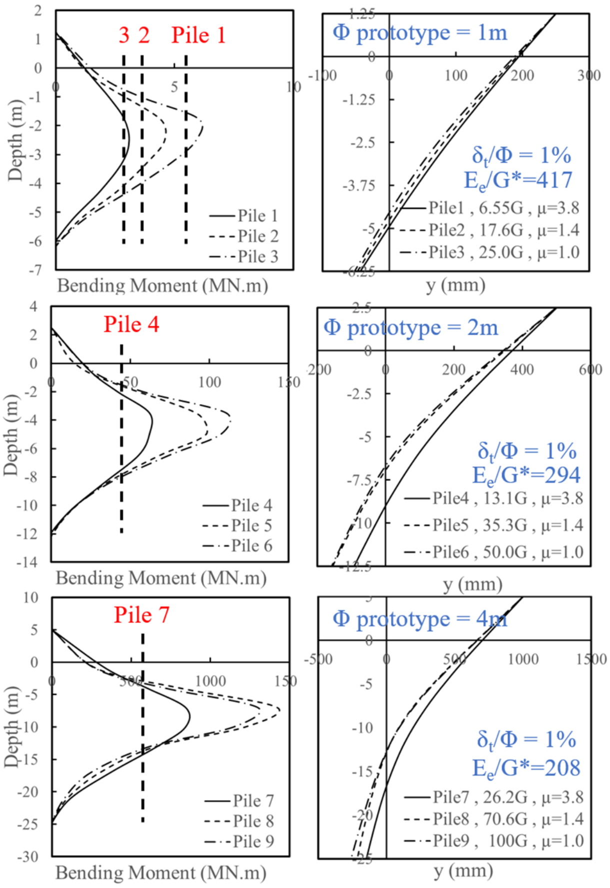

Figure 22: Pile bending moment (left) and deflection at δ_t/Φ=25% (right) profiles along the depth (GSL applied)

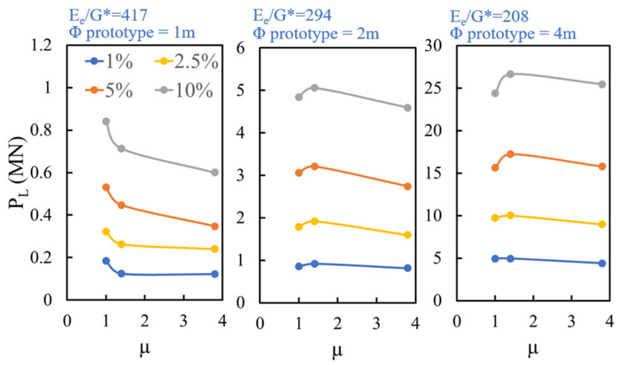

Figure 23: P_L- μ relations

At Ee/G*=417, profiles show minor differences at δ_t/Φ=1%. However, from δ_t/Φ=5%, Pile 1 (μ=3.8) and Pile 2 (μ=1.4) shows lower bending moments compared to Pile 1 (μ=1), even before the theoretical M_y. This challenges the validity of the assumption of stiffness proportional to square root of stress at this pile displacement level. Notably, for all the nine piles, the bending moment differences become much greater once the piles reached M_y at larger δ_t/Φ.

While the bending moment profiles at E_e/G^*=294 and 208 show alignment before reaching M_y, discrepancies are evident at E_e/G^*=417, regardless of the μ and δ_t/Φ values. This suggests a potential incompatibility between GSL and foundations with high E_e/G^*, such as monopiles.

In **Figure 21**, with GSL prototype Φ=4m, a significant divergence occurs around δ_t/Φ = 10%. At this point, both Piles 8 and 9 have surpassed their failure bending moments, exhibiting larger results compared to Pile 7 that has yet to structurally fail. The failure bending moments, marked by dotted straight lines in **Figure 21**, are identified as a critical factor contributing to the overestimation of bending moments.

Furthermore, the center of rotation tends to shift upwards for all GSL cases after exceeding M_y, coinciding the occurrence of pile buckling in **Figure 18**. Specifically, the rotational center naturally moves towards the location of structural failure, and as seen in **Figure 18**, the locations of buckling are considerably higher than those of rotational centers indicated by the deflection profiles in **Figure 21**. In addition, the pile deflection profiles in **Figure 22** agree with **Figure 18** because the locations of structural failure and rotational center move up when μ becomes smaller.

The bending moment profiles in **Figure 22** also agree with **Figure 18**, as Pile 1 is the only one that has not reached M_y, and no buckling is observed. Pile 2, which surpassed M_y in **Figure 22**, did not exhibit visible buckling in **Figure 7**, possibly due to the insufficient plastic deformation to form visually distinguishable buckling.

Comparing where the assumption of $\lambda_\varepsilon=\mu^{0.5}$ in GSL fails (δ_t/Φ = 2~2.5%) in **Figure 20** and where structural failure occurs (around δ_t/Φ = 25% shown in **Figure 10**), it can be said that the results by GSL may not be strictly valid even before structural failures. Furthermore, because no obvious signs of structural failure can be observed in Pile 1 and 2 even beyond δ_t/Φ = 25% in **Figure 9** and **10**, the deflections of them in **Figure 22** do not deviate much from that of Pile 3. It seems like GSL could be acceptable in pile deflection estimation until structural failure occurs using the measured bending moment of pile.

Figure 23 illustrates the effect of μ on pile horizontal loading for various δ_t/Φ. Combining previous observations with **Figure 23**, it can be summarized that: 1) Minimal influence from μ at δ_t/Φ=1%, except for E_e/G^*=417; 2) The the effect of μ is different over δ_t/Φ=2.5%; 3) The effect of μ changes from 1m to 2m of prototype diameter.

4. Conclusions

To assess GSL applicability, centrifuge tests were performed on nine model piles with different wall thicknesses and η to create three E_e/G^* levels, maintaining a constant Φ/d_c. Mechanical behaviors were analyzed using both centrifuge scaling law and GSL to understand the impact of E_e/G^* and structural failure. The conclusions are as follows:

1. The applicability of GSL depends on the level of soil strain along the pile. In this study, GSL shows acceptable results at small pile top displacements, such as δ_t/Φ =1% for E_e/G^*=417, δ_t/Φ =2% for E_e/G^*=294, and δ_t/Φ =2.5% for E_e/G^*=208. The limitation of GSL is particularly pronounced for larger E_e/G^* model piles resembling monopiles.
2. The applicability of GSL also depends on the yielding of pile. Once a pile reaches its M_y, the GSL-estimated P_L-δ_t curves will start to diverge. However, GSL can show limitations before M_y.
3. Increasing μ (1G scaling factor) tends to result in the underestimation of lateral resistance in a single pile before structural failures, highlighting a potential limitation in GSL's core assumption regarding the scaling factor of strain ($\lambda_\varepsilon=\mu^{0.5}$).
4. The location of structural failure tends to shift upward as μ decreases, attributed to the relatively smaller soil confinement compared to the GSL estimation.

References

Arany, et al., 2017. Design of monopiles for offshore wind turbines in 10 steps. Soil Dynamics and Earthquake Engineering, 92, pp.126-152.

API (American Petroleum Institute), 2011. Recommended practice 2GEO geotechnical and foundation design considerations. Washington, DC: API.

Iai, S. et al., 2005. Generalised scaling relations for dynamic centrifuge tests. Geotechnique, 55(5), pp. 355-362.

Iwasaki, T., et al., 1978. Shear moduli of sands under cyclic torsional shear loading. Soils and foundations, 18(1), pp. 39-56.

Tobita, T., & Iai, S., 2011. Application of the generalized scaling law to liquefiable model ground. Stress, 20(10.0), 2-00, pp. 225-236.

Tobita, T., & Iai, S., 2016. New modelling of models for dynamic behavior of a pile foundation. Japanese Geotechnical Society Special Publication, 2(33), pp. 1200-1203.

Klinkvort, R. T., et al., 2013. Scaling issues in centrifuge modelling of monopiles. International Journal of Physical Modelling in Geotechnics, 13(2), pp. 38-49.

Klinkvort, R.T. et al., 2018. A review of modelling effects in centrifuge monopile testing in sand, 9th ICPMG, London, pp.719-724.

Randolph, M. F., 1978. Theoretical study of the performance of piles (Doctoral dissertation).

Randolph, M. F., 1981. The response of flexible piles to lateral loading. Geotechnique, 31(2), pp. 247-259.

Wang, H., et al., 2023. Lateral behavior of monopiles in sand under monotonic loading: Insights and a new simple design model. Ocean Engineering, 277, 114334.